# HIGH RESOLUTION IMAGING OF PRESSURISED WATER SUPPLY LINES

Saber Nasraoui[1] Moez Louati[2], Mohamed Salah Ghidaoui[2]

[1]Department of Water Supply, Sanitation and Environmental Engineering, IHE Delft, Netherlands.
[2]Department of Civil and Environmental Engineering, Hong Kong University of Science and Technology, Clear Water Bay Campus, Hong Kong

## Abstract

This paper proposes a computationally efficient, nondestructive, and long-range guided wave imaging of pressurized water supply lines based on the time reversal (TR) technique. A send-receive transducer is inserted in the water column from a single access point and used to measure multi-input-multi-output (MIMO) pressure wave signals that propagate along the waveguide. The resulting high frequency (10kHz-100kHz) signals are processed by the TR-MUltiple SIgnal Classification (TR-MUSIC) algorithm to provide high-resolution images of tens to hundred of meters long sections of a pipeline in the either side of the transducer. The resulting images reveal the pipe wall inner and outer condition with millimeter resolution. The proposed technique is tested and validated in lab as well as in field scale facilities on pressurized water-filled viscoelastic high-density polyethylene (HDPE) pipes. In particular, we successfully imaged (i) a straight 6.5 m long, water-filled 90 mm HDPE lab pipe containing a small blockage with thickness 7.65 mm and a length 97 mm and (ii) a 36.5 m long section water-filled 160 mm HDPE pipe containing three T-connections and a small blockage with thickness 16 mm and length 95 mm.

**Key words**: Acoustic imaging; time reversal; high-frequency acoustic waves; pipeline; water supply.

Preprint not peer reviewed

This preprint research paper has not been peer reviewed. Electronic copy available at: https://ssrn.com/abstract=4841303

# 1. Introduction

Urban Urban Water Supplies Systems (UWSS)—a complex network of pipes that lie beneath our streets—are vital for life and economic productivity. Such systems often experience the formation of defects during their lifetime due to physical and/or chemical processes, including corrosion, failure of pipe lining, and deposition of suspended fine particles. Such defects often begin as a cluster of small defects on the inside of a pipe wall which we refer to hereafter as incipient defects. The growth of such incipient defects with time can eventually lead to bursts, leaks, and sizeable blockages, resulting in unacceptably large system water losses and excessive energy use. Recent studies estimate that 126 billion cubic meters are unaccounted for annually by water utilities around the world, for an equivalent monetary loss of USD 39 billion [1]. Until now, efforts to curb these massive water losses and energy wastage in existing UWSS has focused on non-intrusive and non-destructive technology development for detecting existing, fully-fledged, physical defects and operational inefficiencies. However, pinpointing incipient defects at an early stage for remediation prevents them from further developing to an extent where they can cause severe operational problems and notable damages in pipes.

Internal sensor-based imaging systems are used to monitor and report the condition of a pipeline's internal surface and pipe wall and enable detection of corrosion sites, cracks, wall thickness, and weld condition, as well as existing leaks. Smart Pipeline inspection gauges (Smart PIGs) were originally developed by the energy pipeline industry and have only recently been emulated by water pipe tools like Smart Ball, Sahara, CCTV, and acoustic sonar [2, 3, 4]. These tools may also have on-board optical, magnetic, or acoustic sensors which, like Smart PIGs, must be launched into a water pipe and be retrieved through a suitably sized port, sometimes using a tether cable. PIG-based sensors are not autonomous or semi-autonomous (even in the energy pipeline sector);

Preprint not peer reviewed

This preprint research paper has not been peer reviewed. Electronic copy available at: https://ssrn.com/abstract=4841303

rather, they are propelled by the pipe flow or tethered. This technology is suitable for use in conduits that present no obstructions to free passage of in-line sensing tools (e.g., oil & gas pipelines). On the other hand, UWSS are often intricate networks of pipes with numerous pipe-diameter changes, partial-bore inline valves and abrupt changes in direction that do not permit the use of inline Smart PIGs. In addition, inline Smart PIGs are currently a slow, in-pipe, survey process (device travels at ~ 0.3 m/s) that cannot support real-time imaging. Moreover, inline Smart PIGs involve significant costs and labor, require traffic diversion and cannot solve defects with separation of the order of ~ 80 cm and below [2].

Less costly, non-disruptive, and more efficient techniques such as transient (acoustic)-based defect detection methods (TBBDM) have been intensively studied and developed [5, 6, 7, 8, 9, 10, 11, 12, 13]. Among these methods, the low frequency (< 100 Hz) wave-based methods are unique for their fast speed (~1000 times faster than roving sensors) and broad coverage (~kilometres), are both economical and applicable to all fully-developed faults. However, low frequency (LF) wave-based methods have poor location resolution (tens to hundreds of metres [6]) and are limited to defects which are large enough to produce visible reflections since noise is strong at the LF band. Since the achievable resolution is directly proportional to the probing wavelength, high frequency (HF) wave-based methods have been developed to achieve a resolution in the order of centimeters [14, 15]. Yet, these HF wave-based methods remain applicable only for fully fledged defects (i.e., through-wall defects such as leaks and also defects with a radial length scale of the order of 15% of the pipe diameter or larger).

The imaging would permit UWSS management to move from reactive to proactive mode, where anomalies with length scales of the order of millimetre are detected and imaged (not just 3ocalized) using high frequency acoustic waves (in the range of 10 to 100 kHz). The proposed imaging

Preprint not peer reviewed

This preprint research paper has not been peer reviewed. Electronic copy available at: https://ssrn.com/abstract=4841303

technique serves as a decision support tool for timely maintenance and mitigation measures. The produced image can reveal the pipe wall inner and outer condition, incipient as well as existing defects at a scale up to millimeters and small (5 to 10%) change in wall stiffness or mass. The proposed pipeline imaging technique is based on the wave time reversal property that has been experimentally proven in UWSS [16]. The proposed method involves a forward step where actively-generated high frequency waves in UWSS are sensed, followed by a Time Reversal step where the chronological order of the subspace noise is reversed and re-emitted into a model of the UWSS. The proposed technique is tested and validated in lab as well as in filed scale facility comprised of pressurized water-filled viscoelastic HDPE pipes.

## 2. Fundamental principle and Time-Reversal imaging algorithm

Consider a water-filled pipe with a cross section of radius $R$ as sketched in Figure 1. We use the cylindrical coordinates, $(x, r)$, where $r$ is defined along the radius in the pipe cross section and the cylindrical coordinate $x$ is defined along the cylinder axis.

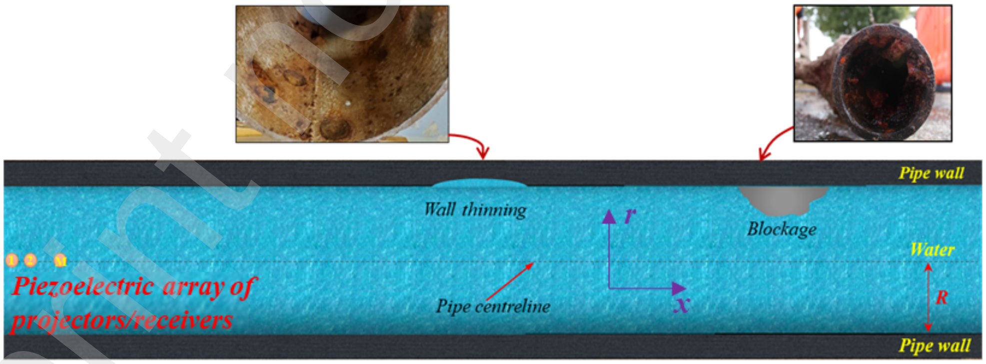

Figure 1: Sketch of a water-filled pipe system containing multiple defects and a piezoelectric array. It shows the location of M-piezoelectric sensor array along the pipe centerline axis. The

Preprint not peer reviewed

This preprint research paper has not been peer reviewed. Electronic copy available at: https://ssrn.com/abstract=4841303

piezoelectric elements are used not only as transmitters but also as receivers. Each element in the piezoelectric array is excited in turn, and all the array elements receive response signals.

## 2.1. Multistatic Response Matrix

The MIMO data is obtained via an array of transducers in which the complete set of time-domain signals for every pair of transmitter-receiver elements in the array is collected. Figure 1 shows the locations of $M$-transducers array placed along the pipe centerline denoted as $\boldsymbol{x_e} = (x_e, r_e)$ where $x_e$ and $r_e$ represent respectively the axial and the radial coordinates of the $e^{\text{th}}$ location, and $e = 1, 2, ..., M$. The data is collected as follows: at each of the $e^{\text{th}}$ transducer location, an acoustic source signal $S(t)$ is projected, and the system response is measured at all locations within the array at a sampling rate $F_s$ (as the rule of thumb, the $F_s$ is ten times the maximum injected frequency). The *collected time-domain* signals $P(n/F_s, \boldsymbol{x}_i \,|\, \boldsymbol{x}_j)$ from each transmitter–receiver combination are grouped into a $(M{\times}M{\times}N)$ 3D matrix $\mathbf{K}_{3D}$ (Figure 2) where $I = 1, 2, ..., M$, $j =1, 2, ..., M$, $n =1, 2, ..., N$, and $N$ is the signal length in time, $\boldsymbol{x}_j$ is the source location and $\boldsymbol{x}_i$ is the receiver location.

This paper focuses on imaging with high frequency (10kH-100kHz). The low level of noise in this frequency range [17] allows the use of the single-frequency versions of the TR-MUSIC algorithms and develop real time pipe imaging technique. In practice, the multistatic response matrix $\mathbf{K}(\omega)$ is built from the 3D matrix $\mathbf{K}_{3D}$ using fast Fourier transforms (FFTs) and the result is $\hat{\mathbf{K}}_{3D}$. For example, when using a Gaussian modulated sine pulse acoustic source, the imaging technique will be applied for every $\mathbf{K}(\omega_0)$, where $\omega_0$ is the central frequency of the injected source and at which the frequency response signal peaks.

Preprint not peer reviewed

This preprint research paper has not been peer reviewed. Electronic copy available at: https://ssrn.com/abstract=4841303

## 2.2. Time-Reversal Operation

In this paper the MUSIC approach for time-reversal imaging is considered. This approach was first proposed in [18] and named 'time-reversal MUSIC' because both time-reversal methods [19]and MUSIC can be explained using the eigenvalues of the time reversal operator [20]. The theory of generalized TR-based imaging methods depends on the ability to perform a singular value decomposition (SVD) of the multistatic response matrix or an eigenvalue decomposition (ED) of the time-reversal matrix. In the following the SVD approach is used.

### i) *Singular Value Decomposition:*

Consider the singular value decomposition (SVD) of $\mathbf{K}(\omega_0)$:

$$\mathbf{K}(\omega_0) = \mathbf{U\Sigma V}^H \tag{1}$$

where the superscript '$H$' is the conjugate transpose, **U** and **V** are matrices whose columns are the singular vectors $\boldsymbol{\mu}_i$ and $\boldsymbol{v}_i$, while $\boldsymbol{\Sigma} = \mathrm{diag}\{\sigma_1, \sigma_2, \ldots, \sigma_{\mathrm{M}}\}$, is a diagonal matrix with singular values $\sigma_i$, arranged in order of decreasing magnitude. The singular vectors $\boldsymbol{\mu}_i$ and $\boldsymbol{v}_i$ belong each to a signal and a noise subspace. In practice, because of the presence of experimental noise, additional singular values may become significant, which makes it difficult to distinguish the signal and noise subspaces. In these cases, a threshold criterion can be chosen to divide the signal subspace from the noise subspace [21]. The value of this threshold is empirical and so should be tuned depending on the system and defects of interest. Here, in the case of pipe system imaging a threshold of 10% of the maximum singular value at each frequency was found to give accurate blockage image. The sensitivity of the chosen threshold (10%) is addressed, and the results provide that for a perturbation of a few percent, the output TR-MUSIC blockage image remains unchanged. Under the threshold criterion the signal and noise components are extracted extract as follows: **U**= [$\mathbf{U}_{\mathrm{signal}}$

Preprint not peer reviewed

This preprint research paper has not been peer reviewed. Electronic copy available at: https://ssrn.com/abstract=4841303

|$\mathbf{U}_{\text{noise}}$] = [$\boldsymbol{\mu}_1$, $\boldsymbol{\mu}_2$,..., $\boldsymbol{\mu}_m$| $\boldsymbol{\mu}_{m+1}$,..., $\boldsymbol{\mu}_M$] and $\mathbf{V}$=[$\mathbf{V}_{\text{signal}}$ |$\mathbf{V}_{\text{noise}}$] = [$\boldsymbol{v}_1$, $\boldsymbol{v}_2$,..., $\boldsymbol{v}_m$| $\boldsymbol{v}_{m+1}$,..., $\boldsymbol{v}_M$]. where, $\mathbf{U}_{\text{signal}}$ and $\mathbf{V}_{\text{signal}}$ are the left and right signal subspaces, $\mathbf{U}_{\text{noise}}$ and $\mathbf{V}_{\text{noise}}$ are the left and right noise subspaces, and $m$ is the number of columns of the signal subspaces matrix, which is threshold dependent.

### ii) ***Imaging function:***

A first-order Newmann series solution is considered to obtain the theoretical model for multi-scatterers in a pipe system where weak scattering strength is assumed [22, 23]. Consequently, the theoretical singular vector ($\boldsymbol{\mu}^{Model}$) from the signal subspace associated to an arbitrary scatterer at $\boldsymbol{x_{sc}}$=($x_{sc}$, $r_{sc}$) can be written as :

$$\boldsymbol{\mu}^{Model}(\omega_0, \boldsymbol{x}_e \,|\, \boldsymbol{x}_{sc}) = [G(\omega_0, \boldsymbol{x}_1 \,|\, \boldsymbol{x}_{sc}), G(\omega_0, \boldsymbol{x}_2 \,|\, \boldsymbol{x}_{sc}), ..., G(\omega_0, \boldsymbol{x}_M \,|\, \boldsymbol{x}_{sc})]^T \qquad (2)$$

where $G$ is the Green's function of the pipe system medium defined as [24, 25]

$$G\left(\omega_0, \boldsymbol{x}_e \,|\, \boldsymbol{x}\right) = \frac{i}{2\pi} \sum_{\eta} \frac{J_0\left(k_{r\eta} r_e\right) J_0\left(k_{r\eta} r\right)}{R k_{x\eta}\left(1 - \dfrac{\omega_0^2}{R^2 k_{r\eta}^2 Z^2(\omega_0, k_{r\eta})}\right) J_0^2\left(R k_{r\eta}\right)} \exp\left(-i k_{x\eta} \,|\, x_e - x \,|\right) \qquad (3)$$

$G(\omega_0, \boldsymbol{x}_e \,|\, \boldsymbol{x})$ represents the system impulse response at $\boldsymbol{x}_e$ given a source at $\boldsymbol{x}$, for a given frequency $\omega_0$, and comprises the sum of multiple propagating modes $\eta$, each described by the modal axial and radial wavenumbers, $k_{x\eta}$ ($\omega_0$) and $k_{r\eta}$( $\omega_0$), respectively. $J_0$ is the Bessel function of the first kind of order zero, and $Z(\omega_0, k_{r\eta}, )$ is the impedance of the pipe wall, which is evaluated using the shell theory model [14, 26]. Given the orthogonality property between the signal and noise subspaces, the scatterers locations ($\boldsymbol{x_{sc}}$) are associated with the locations $\boldsymbol{x}$ at which the inner product between the green function vector $\boldsymbol{g}(\omega_0, \boldsymbol{x}_e \,|\, \boldsymbol{x})$ =[$G(\omega_0, \boldsymbol{x}_1 \,|\, \boldsymbol{x})$, $G(\omega_0, \boldsymbol{x}_2 \,|\, \boldsymbol{x})$,…,$G(\omega_0, \boldsymbol{x}_M \,|\, \boldsymbol{x})$

Preprint not peer reviewed

This preprint research paper has not been peer reviewed. Electronic copy available at: https://ssrn.com/abstract=4841303

$]^T$ and the noise subspace ($\boldsymbol{\mu}_i$ ($i = m+1,\ldots, M$)) is zero, where $\boldsymbol{x}=(x, r)$ scans the whole pipe domain space. Thus, the imaging function $\varphi(\boldsymbol{x}, \omega_0)$ can then be constructed as follows

$$\varphi(\boldsymbol{x},\omega_0)=\left[\sum_{i=m+1}^{M}|<\boldsymbol{\mu}_i,\boldsymbol{g}(\omega_0,\boldsymbol{x}_e\,|\,\boldsymbol{x})>|^2\right]^{-1} \tag{4}$$

where the strength of $\varphi(\boldsymbol{x}, \omega_0)$ at different $\boldsymbol{x}$ provide the pipe local image corresponding to the measured transfer matrix $\mathbf{K}(\omega_0)$. The set of $\boldsymbol{x}$ values where $\varphi(\boldsymbol{x}, \omega_0)$ is maximum provides the special region that defines the scatterers (i.e. defects in the pipe).

### iii) ***Local Imaging function:***

TR-MUSIC has a poor capability of detecting multiple scatterers, especially when the number of the sensor array is small [27]. In order to deal with the forgoing issue, an enhanced monitoring strategy based on the local TR-MUSIC algorithm [28] is applied. This means that the acoustic response from the pipe system is split into a set of sub-responses. Each sub-response presents the scattered signal from a local region in the pipe. In addition, since the scattered signals of different time periods are cut out for a local region processing from zero, this is equivalent to scanning the pipe domain from near to far according to the distance from the location of the receiver. The process of the local TR-MUSIC algorithm is similar to the short-time Fourier transform. First, a moving Hanning window (MHW) in time is applied to $\mathbf{K}_{3D}$ to obtain a set of 3-D local matrices $\mathbf{K}^{\ell}{}_{3D}$ where $\ell = 1, 2,\ldots, \mathrm{I}$, and $\mathrm{I}=N/t_c$ of the MHW (see Figure 2) [28]. Second, each local matrix $\mathbf{K}^{\ell}{}_{3D}$ is transformed in the frequency domain using the Fast Fourier transform (FFT) and the result is $\hat{\mathbf{K}}^{\ell}_{3D}$ that perform the local multistatic response matrix $\hat{\mathbf{K}}^{\ell}(\omega_0)$ and thus it's local singular value decomposition. Thus, there exists $t_c$-dependent singular value decomposition nonzero singular

Preprint not peer reviewed

This preprint research paper has not been peer reviewed. Electronic copy available at: https://ssrn.com/abstract=4841303

values. Herein, the $t_c$ is chosen so that the number of scatterers (i.e., the number nonzero singular values) does not exceed the total number of sensing array elements.

Finally, the time reversal operation is applied to every frequency-transformed local matrix for a given frequency $\hat{\mathbf{K}}^{\ell}(\omega_0)$ (local multistatic response matrix), performing a set of imaging functions $\varphi^{\ell}(\boldsymbol{x},\ \omega_0)$. The full pipe imaging function $\varphi\,(\boldsymbol{x},\ \omega_0)$ is obtained by summing all local imaging functions $\varphi^{\ell}(\boldsymbol{x},\ \omega_0)$ for $\ell = 1, 2, \ldots, I$, which is written as

$$\varphi(\boldsymbol{x},\omega_0) = \sum_{\ell} \varphi^{\ell}(\boldsymbol{x},\omega_0) \qquad (5)$$

The strength of $\varphi(\boldsymbol{x},\ \omega_0)$ at different $\boldsymbol{x}$ provides the full pipe image.

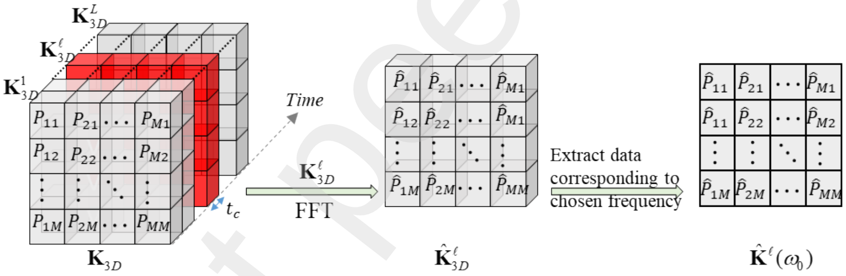

Figure 2: Experimental transfer matrix arrangement.

## 3. Testing the Proposed Imaging Method Using Synthetic data

### 3.1. Noise-free synthetic data: rigid pipe case

This section provides an example to verify the effectiveness and feasibility of the developed TR-based imaging algorithm using synthetic data generated by the analytical model developed in Ref ( [14]). The test case consists of an unbounded rigid pipe with radius R=0.0393 m containing a small blockage located 2.36 m away from the sensors array (see Figure 3). The blockage was

Preprint not peer reviewed

This preprint research paper has not been peer reviewed. Electronic copy available at: https://ssrn.com/abstract=4841303

simulated in the two-dimensional pipe domain by aligning closely 70 spaced scattering points. In this example the MIMO data is obtained via an array of 10 transceivers placed along the pipe centerline and spaced every 2 cm. The simulated blockage is drawn with small dots ( Figure 3. b) and the array of 10 transceivers is drawn with small circles ( Figure 3. a).

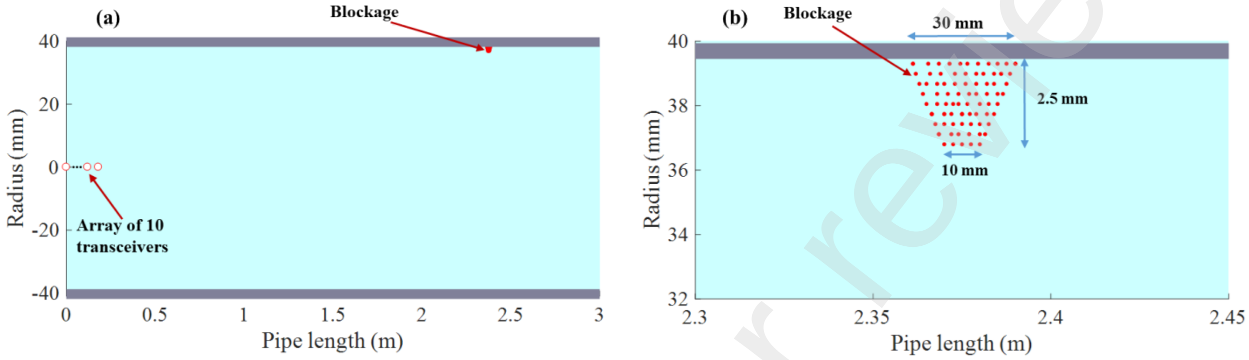

Figure 3: (a): Sketch of the considred pipeline system for imaging. (b): Zoomed version.

The wave speed is assumed to be constant at 1480 m/s. The excited wave source signal $S(t)$ is a Gaussian-modulated sine wave with central frequency $f_0$ =55 kHz (or $\omega_0 = 2\pi f_0$) and a narrow frequency bandwidth FBW= $[0.9f_0$ to $1.1f_0]$ (i.e. the minimum probing wavelength $\lambda \sim 2.4$ cm ) [29, 30]. The sampling rate is 1 MHz, and the length of the time signal of the system response is set to T = 0.01 s, which is enough to capture the reflection from the blockage. Figure 4.a shows the scattered signal received by the 10th sensor (i.e., the one nearest to the blockage) when the source is at the first position of the transducers array.

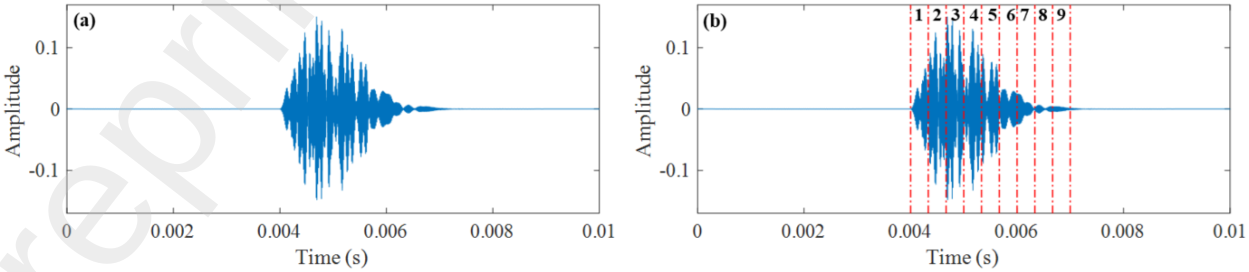

Preprint not peer reviewed

This preprint research paper has not been peer reviewed. Electronic copy available at: https://ssrn.com/abstract=4841303

Figure 4: Scattered signal received by the 10th sensor when the source is acting on the first transducers array.

In this test case the number of the sensor array (10 sensors) is smaller than the number of the scatterers (70 scattering points). Therefore, the local TR-MUSIC algorithm is applied. The time interval $t_c$ of the Hanning window is taken to be T/30 in order to ensure that the number of scatterers is smaller than the number of transducer elements (i.e., 10). Moreover, one can choose $t_c$ smaller than T/30, but this increases the time of the imaging computation without gain in terms of accuracy. In fact, a Hanning window with $t_c$= T/40, and $t_c$= T/60 has also been applied (not shown here for brevity), and the imaging accuracy is the same as the T/30 case.

For the time window interval $t_c$= T/30=(0.01/30)s, the scattered signal is divided into 30 sub-scattered signals in which there are nine signals with significant amplitudes (see Figure 4.b). From each received signal, nine sub-scattered signals caused by the blockage are subtracted, then the resulting nine transfer matrices are substituted into the TR-MUSIC algorithm, performing nine imaging functions $\varphi^{\ell}(\boldsymbol{x}, \omega_0)$, $\ell = 1, 2, \ldots, 9$ plotted in Figure 5. Combining Figure 5.1)–(5.9) gives the accurate image of the blockage in the considered pipe system (see Figure 4).

Preprint not peer reviewed

This preprint research paper has not been peer reviewed. Electronic copy available at: https://ssrn.com/abstract=4841303

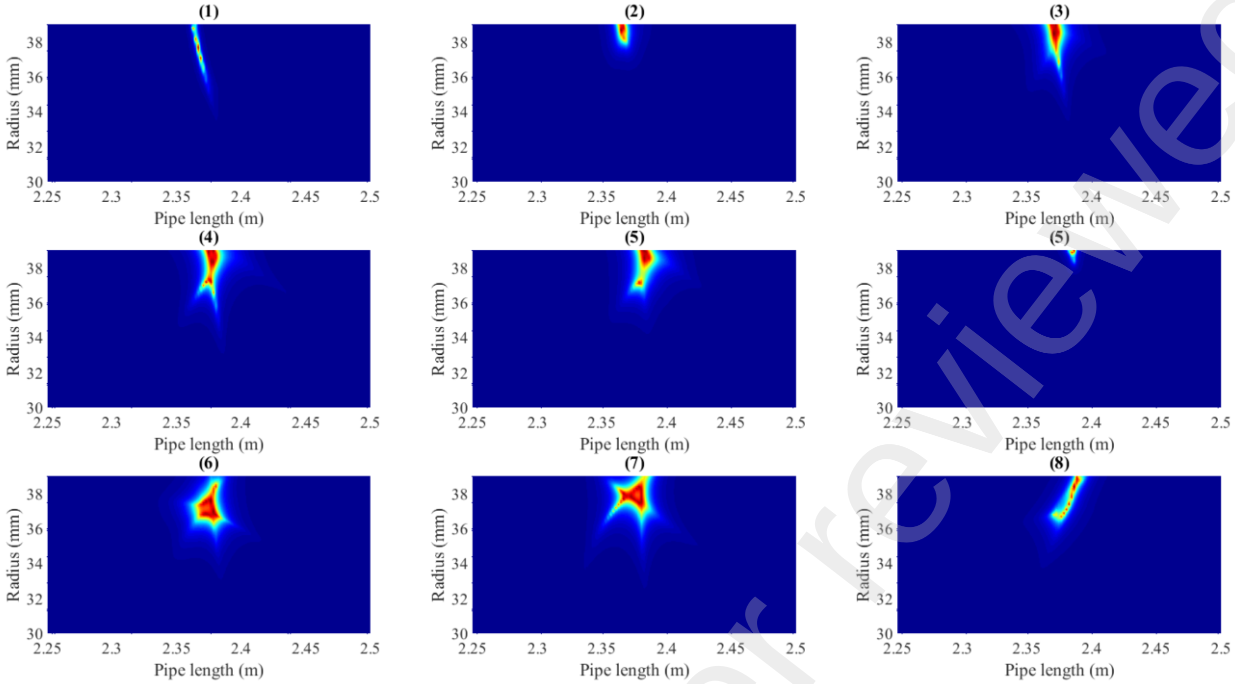

Figure 5: Local TR-MUSIC images  when a Hanning window with width equal to T/30 = (0.01/30)s is applied to the original signal.

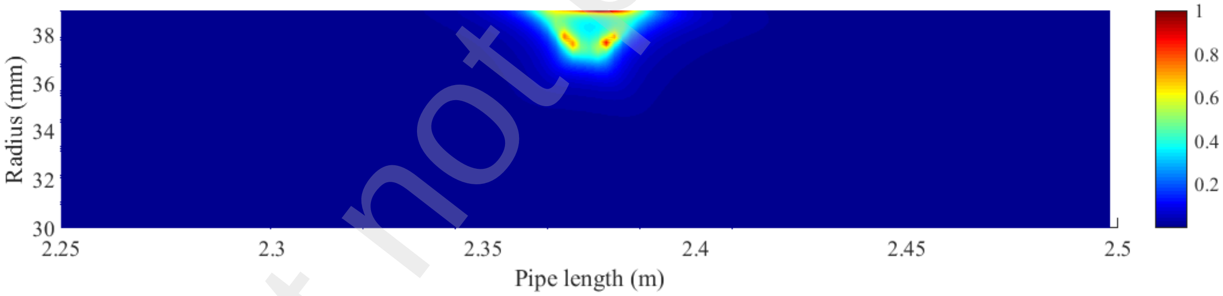

Figure 6: Combination of the Local TR-MUSIC images.

### 3.2. Effect of noise: rigid pipe case

A zero-mean Gaussian white noise is added to the synthetic data of the previous test case. Therefore, the multistatic response matrix can be written in the form

$$\mathbf{K}' = \mathbf{K} + \mathbf{N} \quad (6)$$

Preprint not peer reviewed

This preprint research paper has not been peer reviewed. Electronic copy available at: https://ssrn.com/abstract=4841303

where **K** is the noise-free multistatic response matrix and **N** is the added zero mean complex Gaussian noise matrix. The signal-to-noise ratio (SNR) in decibels is defined by

$$\mathrm{SNR} = 20\log_{10}\left(\frac{\|\mathbf{K}'\|}{\|\mathbf{N}\|}\right) \tag{7}$$

where ||.|| is the usual $L_2$ matrix norm.

Figure 7 shows the pipe image of the considered blockage, computed from a single realization of noisy data having a signal-to-noise ratio of roughly 22 dB. The effect of the noise is evident from the Fig. 7 in the form of spurious maxima surrounding the maxima due to the blockage locations. In addition, the blockage image as estimated from the time reversal MUSIC has an error in the location and shape of the blockage. The fact that we considered only the most restrictive case of single snapshot data explains why large errors occur (Figure 1(b)) at relatively low noise levels. To address the noise issue, we conduct the blockage imaging with multiple realizations of noisy data and find that after 20 realizations the output time reversal image remain unchanged. The result of 20 realizations is plotted in Figure 1 and shows more accurate image. Clearly, the performance can be better, in practice, if one records more than a single realization sample because different noise contributions will statistically cancel out.

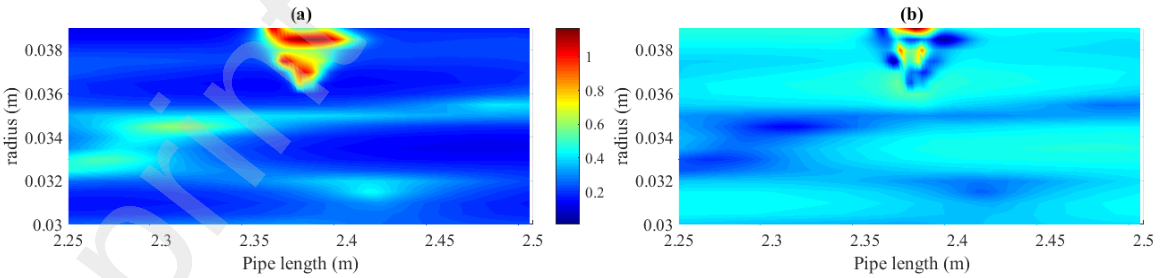

Figure 7: (a): Plots of the time reversal MUSIC blockage image computed from a single realization noisy synthetic data yielding a signal-to-noise ratio of about 22 dB. (b) Difference between signals for noise-free case.

Preprint not peer reviewed

This preprint research paper has not been peer reviewed. Electronic copy available at: https://ssrn.com/abstract=4841303

.

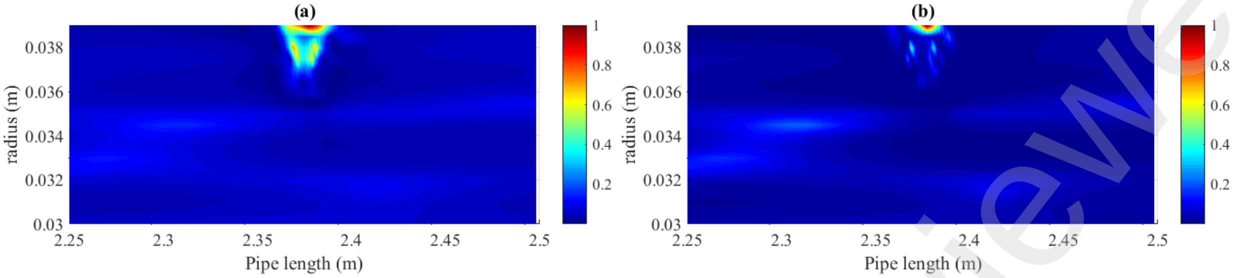

Figure 8: (a): Plots of the time reversal MUSIC blockage image computed from a 20 realizations noisy synthetic data yielding a signal-to-noise ratio of about 22 dB. (b) Difference between signals for noise-free case.

To quantitatively estimate the effect of the noise on the proposed pipe imaging methods, we consider the pipe image of the pipe in free noise case (Fig. 9) as reference image since it produces accurately the actual blockage. Then for given SNR the imaging error induced by the noise is evaluated with respect to the reference image. Here, the relative error $e_{x,r}$ is defined by

$$e_{x,r} = \frac{1}{2}\left( \frac{\| \overline{\boldsymbol{\varphi}}_x(\mathrm{SNR}) - \boldsymbol{\varphi}_x(\mathrm{SNR{=}0}) \|}{\| \boldsymbol{\varphi}_x(\mathrm{SNR} = 0) \|} + \frac{\| \overline{\boldsymbol{\varphi}}_r(\mathrm{SNR}) - \boldsymbol{\varphi}_r(\mathrm{SNR} = 0) \|}{\| \boldsymbol{\varphi}_r(\mathrm{SNR} = 0) \|} \right) \times 100 \qquad (8)$$

Where $\boldsymbol{\varphi}_x$ and $\boldsymbol{\varphi}_r$ are the projections of the imaging function $\boldsymbol{\varphi}$ along $x$ and $r$ axis, respectively, and the overline stands for the average. For each SNR value, 20 noise imaging realizations are generated and the relative error between the actual and the ensemble averaged estimated projections of the imaging function $\boldsymbol{\varphi}$ along $x$ and $r$ axis are computed. Figure 10 depicts the errors for different SNR considering the blockage explored in the previous section. Figure 7 Clearly shows that the accuracy of the blockage image increases as the SNR increases. Therefore, in practice, such experiment requires accurate equipment and low-noise amplifier to achieve accurate results. This will be further discussed in the experimental section below.

Preprint not peer reviewed

This preprint research paper has not been peer reviewed. Electronic copy available at: https://ssrn.com/abstract=4841303

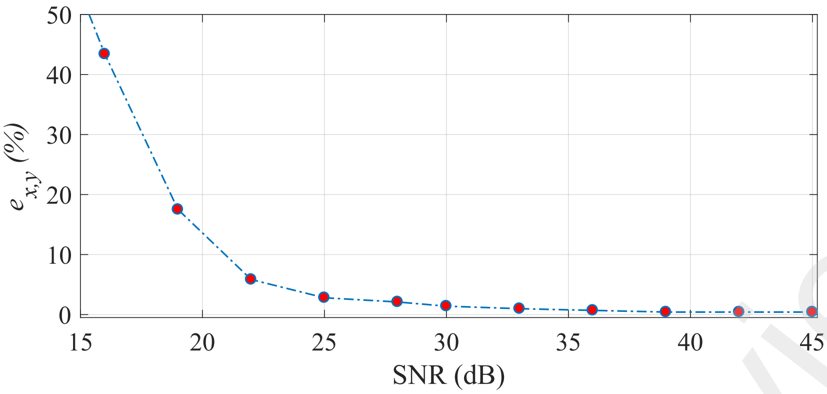

Figure 10: Imaging error of the blockage sketched in fig.3 with respect to SNR (16,19, 22, 25, 28, 30, 33, 36, 39, 42, 45 dB). The central frequency of the Gaussian source is $f_c$ = 55 kHz.

### 3.3. Synthetic data for elastic pipe case

The proposed method has also been applied for elastic pipe wall test case, and the same geometric parameters of the above numerical example are considered for SNR = 30 dB. The analytical model ( [14]) is used to generate synthetic data to test and demonstrate the imaging algorithm in elastic pipe. Three test defect cases are considered, namely (i) internal wall thinning; (ii) stiffness reduction in a small region along the wall; and (iii) external wall thinning. In each case, the defect is located 20m away from the sensors array. The defect sizes and shapes are shown in Figures 11a, 11c, and 11e. In all test cases, the pipe is considered unbounded, 7.86cm in diameter, 5.7mm in thickness, and viscoelastic in material (same as HDPE parameters).

Preprint not peer reviewed

This preprint research paper has not been peer reviewed. Electronic copy available at: https://ssrn.com/abstract=4841303

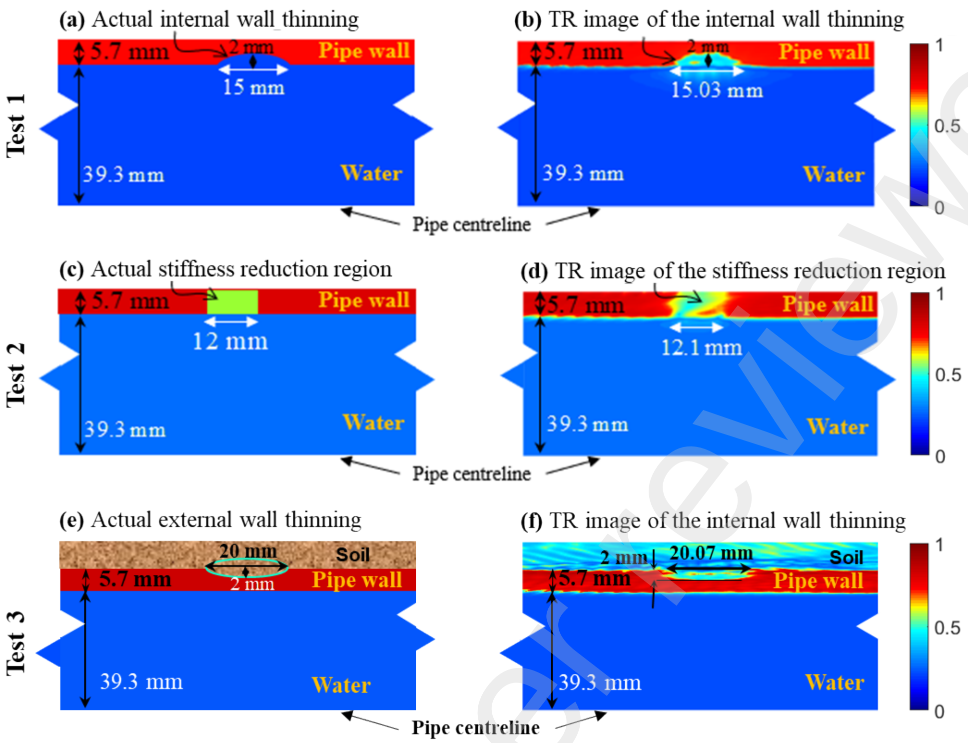

Figure 11: TR image (a-b) internal pipe wall thinning, (c-d) 10% reduction in stiffness, and (e-f). The probing central frequency $f_0$ = 70 kHz.

The MIMO data is obtained via an array of 10 transceivers placed along the pipe centerline and spaced by 2 cm. The excited wave source signal $S(t)$ is a Gaussian-modulated sine wave with central frequency $f_0$ =70 kHz (or $\omega_0 = 2\pi f_0$) and a narrow frequency bandwidth FBW= [$0.9f_0$ to $1.1f_0$] [29, 30]. The sampling rate is 1 MHz, and the length of the time signal is set to T = 0.02 s. The Hanning window width is taken as T/20. Applying the proposed imaging algorithm described in the previous section, the pipe images of the three considered test cases are given in Figure 11b, Figure 11d, and Figure 11f. Figure 11 compares the identified TR image of the defect location, size, and shape, as well as the pipe wall and its thickness, with the actual cases and shows accurately predicted TR images.

Preprint not peer reviewed

This preprint research paper has not been peer reviewed. Electronic copy available at: https://ssrn.com/abstract=4841303

# 4. Testing the Proposed TR Imaging Method Using Experimental data

## 4.1. Application in Lab facility

The proposed technique for pipeline imaging is experimentally tested in the Water Resources Research Laboratory at Hong Kong University of Science and Technology (HKUST). The experimental setup consists of a straight 6.5 m long, 90 mm diameter HDPE pipe that connects two water-filled tanks at its ends (see Figure 12). The nominal external diameter of the pipe is equal to $90\times10^{-3}$ m, and the pipe wall thickness is $5.7\times10^{-3}$m. To emphasize the imaging capability, the experimental setup includes a blockage introduced as a short pipe section located 3.5 m away from the upstream boundary, with a diameter of 33mm, a thickness $r_B$=7.65 mm, and a length $l_B$ =97 mm as shown in Figure 12.

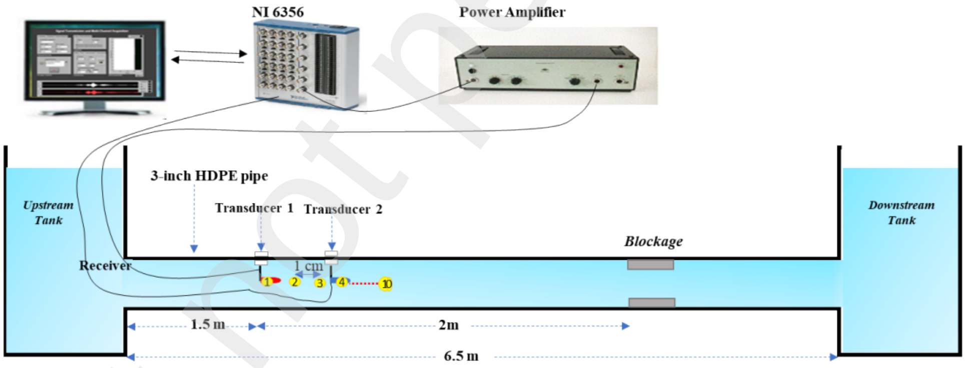

Figure 12: Sketch map of the high-frequency experimental setup in the Water Resources Research Laboratory at HKUST. 3D printed magnetic base is used to mount the transducers inside a 90 mm HDPE pipe with a total length of 6.5 m. A magnet was mounted to drag the transducers. A blockage is deliberately introduced along the pipe. Experiment facilities consisted of a B&K 2713 power amplifier and a NI 6356 data acquisition board.

Preprint not peer reviewed

This preprint research paper has not been peer reviewed. Electronic copy available at: https://ssrn.com/abstract=4841303

An array of 10 transducer locations is considered at the pipe centerline and spaced by 2 cm, and located 1,5 m away from the upstream boundary. Considering a linear wave system, only two Brüel & Kjær Type 8104 transducers are used; one as a projector and the other as a sensor. The multi-input, multi-output (MIMO) data is obtained by successively fixing the projector at a given position in the array and measuring the system response by positioning the sensor successively at all locations within the array. A Gaussian modulated sine wave source $S(t)$ with central frequency $f_0$ =55kHz and a narrow frequency bandwidth FBW= [$0.9f_0$ to $1.1f_0$] is used. The sampling rate is 1MHz, and the length of the measurement time is set to T=0.012 s to prevent the effect of pipe-tank reflection. Prior to data processing, the baseline system response is subtracted to enhance the scattering response signal. The used Hanning window width is one-twentieth the length of the measurement time. Applying the proposed imaging algorithm described in the previous section, the pipe image is successfully given in Figure 13, clearly indicating the blockage location and size as well as the pipe wall and its thickness.

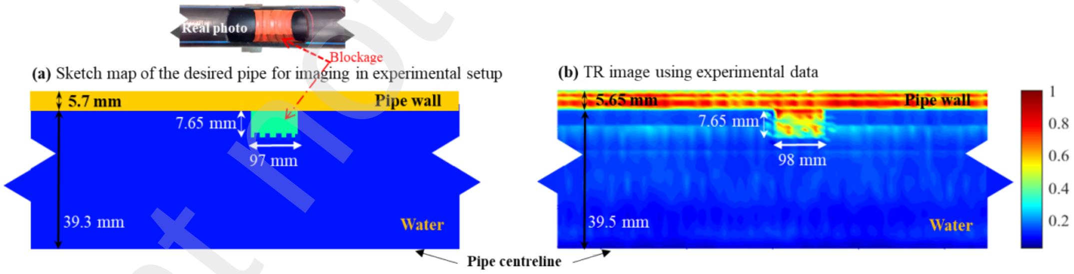

**(a)** Sketch map of the desired pipe for imaging in experimental setup

**(b)** TR image using experimental data

Figure 13: Imaging results of the considered pipeline system. The image is created using the experimental data from the configuration given in Figure 12. The image is computed at $f_0$= 55kHz, and the signal-to-noise ratio SNR=35 dB.

Preprint not peer reviewed

This preprint research paper has not been peer reviewed. Electronic copy available at: https://ssrn.com/abstract=4841303

## 4.2. Application in field-scale facility (Beacon Hill)

The imaging algorithm is further validated in a field-scale facility which represents a more realistic system scale. The facility comprises a 250 m long water-filled viscoelastic 160 mm HDPE pipe (with radius $R$=73 mm) (see Figure 14). A 36.5 m long straight section indicated in Figure 14 is selected to perform the imaging test. The section ends connect to two T-access points from which transducers can be introduced. In this case, the transducers are introduced from the downstream end T-access point (T1). Along this section, three T-connections exist (T2, T3, and T4), and a blockage with a thickness $r_B$=16 mm, and a length $l_B$=95 mm, is introduced at 7m away from the location $x$ = 0 m (see Figure 14).

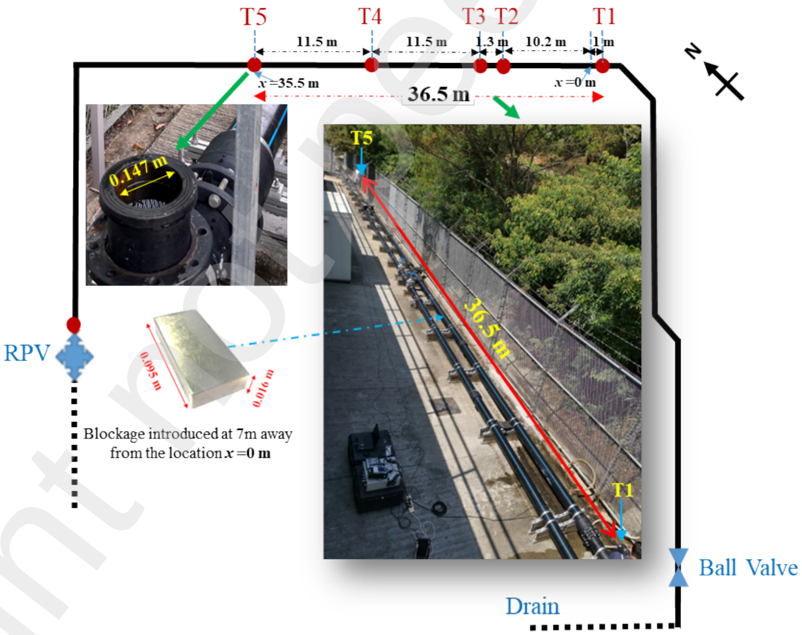

Figure 14: Setup of the pipe transient experiment in Beacon Hill, Hong Kong.

Applying the imaging algorithm and following the measurement technique conducted in the previously described lab case, the pipe section image is provided in Figure 15. The image indicates

Preprint not peer reviewed

This preprint research paper has not been peer reviewed. Electronic copy available at: https://ssrn.com/abstract=4841303

the pipe wall and its thickness, along which three pipe wall openings are shown corresponding to the existing three T-connections. Moreover, the blockage is accurately identified in both location and size.

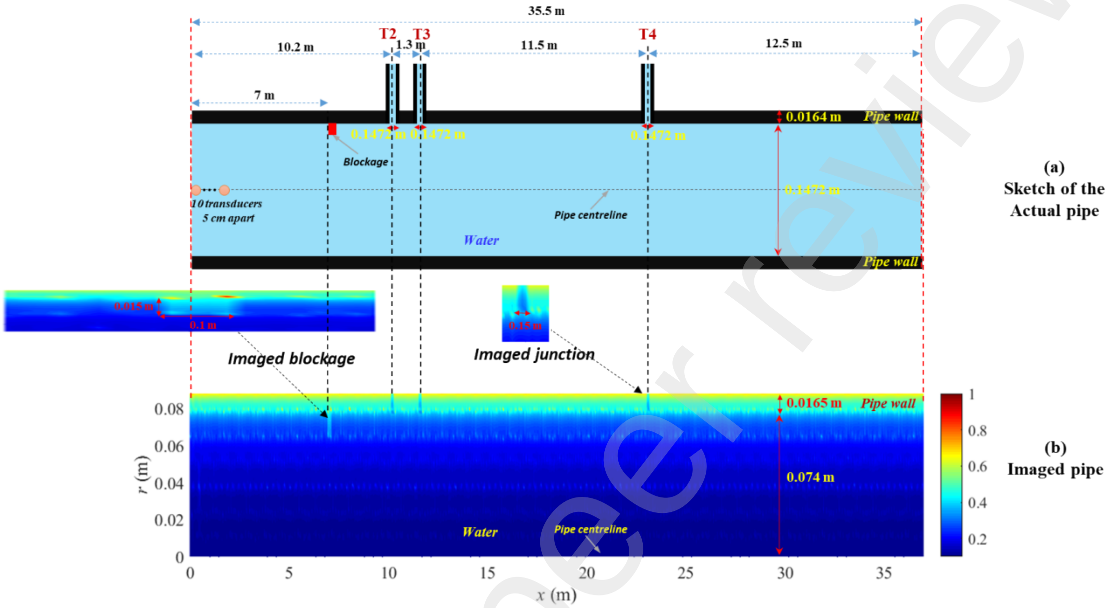

Figure 15: Imaging results of the considered pipeline in Beacon Hill, Hong Kong. The image is computed at $f_0$ = 75kHz, and the signal-to-noise ratio SNR=30 dB.

## 5. Conclusion

This paper proposed a computationally efficient, nondestructive, and long-range guided wave imaging of pressurized water supply lines based on the time reversal (TR) technique. The main conclusion points are:

- The proposed technique is non-disruptive and non-intrusive. It requires a send-receive transducer to be inserted in the water column from a single access point (e.g. an inspection-

Preprint not peer reviewed

This preprint research paper has not been peer reviewed. Electronic copy available at: https://ssrn.com/abstract=4841303

T) and used to measure multi-input-multi-output (MIMO) pressure wave signals that propagate along the waveguide.

- High resolution imaging is achieved using TR-MUSIC in the frequency range of 10kHz to 100kHz. The range of the imaging spans from tens to hundreds of meters long sections of a pipeline in the either side of the transducer.
- The proposed imaging technique is able to reveal the pipe wall inner and outer condition in millimeter scale.
- Both lab and field-scale facilities are used to validate the proposed imaging technique. In the lab, we successfully imaged a straight 6.5 m long, water-filled 90 mm HDPE pipe containing a small blockage with thickness 7.65 mm and a length 97 mm. In the field-scale facility, we accurately imaged a 36.5 m long section water-filled 160 mm HDPE pipe containing three T-connections and a small blockage with thickness 16 mm and length 95 mm.

The development of TR-imaging for water-filled pipelines would permit UWSS management to move from reactive to proactive mode, where anomalies with length scales of the order of millimetre are detected and imaged (not just localised). Thus, it serves as a decision support tool for timely maintenance and mitigation measures.

## References

[1] R. Liemberger and A. Wyatt, "Quantifying the global non-revenue water problem," *Water Supply,* vol. 19, no. 3, pp. 831-837, 2018.

Preprint not peer reviewed

This preprint research paper has not been peer reviewed. Electronic copy available at: https://ssrn.com/abstract=4841303

[2] B. Nestleroth, S. Flamberg, W. Condit, J. Matthews Battelle, L. Wang and A. Chen, "Field Demonstration of Innovative Condition Assesment Technologies for Water Mains: Leak Detection and Location," National Risk Management Research Laboratory - Office of Research and Development - U.S. Environmental Protection Agency, Cincinatti, Ohio, 2012.

[3] "Smartball PWA Inspection Report 16-inch Hanover Park Force Main, prepared by Pure Technologies U.S., Inc., dated November 2015”".

[4] "SmartBall Inspection Report NTW 700mm Pipeline Prepared for Water Supplies Department (Hong Kong) Prepared by Pure Technologies October, 2018".

[5] X. Wang and M.S. Ghidaoui, " "Pipeline Leak Detection Using the Matched-Field Processing Method," , ASCE, 144(6),(2018).," *Journal of Hydraulic Engineering,* vol. 144, no. 6, p. 04018030, 2018.

[6] M. Waqar, M. Loauti and M. S. Ghidaoui, " Time-reversal of water hammer waves," *Journal of Hydraulic Research,* vol. 1, no. 60, pp. 25-45, 2022.

[7] F. Zouari, M. Louati, E. Blåsten and M. S. Ghidaoui, "Multiple defects detection and characterization in pipes," *BHR Group 2018 Pressure Surges 13.*

[8] P.Kumar and P. K. Mohapatra, "Partial Blockage Detection in Pipelines by Modified Reconstructive Method of Characteristics Technique," *J. Hydraul. Eng,* vol. 148, no. 4, p. 04022003, 2022.

[9] A. M. Sattar and H. M. Chaudry, "Leak detection in pipelines by frequency response method," *Journal of Hydraulic Research,* vol. 46, no. sup1, pp. 138-151, 2008.

Preprint not peer reviewed

This preprint research paper has not been peer reviewed. Electronic copy available at: https://ssrn.com/abstract=4841303

[10] S. Kim, "Multiple Discrete Blockage Detection Function for Single Pipelines," *Proceedings,* vol. 2, no. 11, p. 582, 2018.

[11] S. Meniconi, B. Brunone, M. Ferrante, C. Capponi, C. A. Carrettini, C. Chiesa, D. Segalini and E. A. Lanfranchi, "Anomaly pre-localization in distribution–transmission mains by pump trip: preliminary field tests in the Milan pipe system," *Journal of hydroinformatics ,* vol. 17, no. 3, p. 377–389, 2015.

[12] T.C.Che, H. F. Duan and P. J. Lee, "Transient wave-based methods for anomaly detection in fluid pipes," *Mechanical Systems and Signal Processing,,* vol. 160, p. 107874, 2021.

[13] F. Zouari, E. Blåsten, M. Louati and M. S. Ghidaoui, "Internal pipe area reconstruction as a tool for blockage detection," *Journal of Hydraulic Engineering,* vol. 154, no. 6, p. 04019019, 2019.

[14] S. Nasraoui, M. Louati and M. S. Ghidaoui, "Blockage detection in pressurized water-filled pipe using high frequency acoustic waves," *Mechanical Systems and Signal Processing,* vol. 185C, no. 109817, 2022.

[15] S. Nasraoui, M. Louati and M. S. Ghidaoui, "High resolution acoustic identification of clusters of small blockages in fluid-filled pipe using maximum likelihood estimation," *The Journal of the Acoustical Society of America,* vol. 153, no. 5, pp. 3086-3086, 2023.

[16] G. Grigoropoulos, M. S. Ghidaoui, M. Louati and S. Nasraoui, "Time reversal of waves in hydraulics: experimental and theoretical proof with applications," *J. Hydraul. Res,* vol. 1, p. 60, 2022.

Preprint not peer reviewed

This preprint research paper has not been peer reviewed. Electronic copy available at: https://ssrn.com/abstract=4841303

[17] A. Dubey, Z. Li and P. J. a. R. Murch, "Measurement and characterization of acoustic noise in water pipeline channels," *IEEE Access ,* vol. 7, p. 56890–56903, 2019.

[18] H. Lev-Ari and A. J. Devaney, *IEEE Sensor Array and Multichannel Signal Processing Workshop, Cambridge (MA), USA,* p. 509–513, 2000.

[19] C. Prada, S. Manneville, D. Spoliansky and M. Fink, "Decomposition of the time reversal operator: Detection and selective focusing on two scatterers," *J. Acoust. Soc. Am,* vol. 99, p. 2067–2076, 1996.

[20] A. Baussard and T. Boutin, "Time-reversal RAP-MUSIC imaging," *Waves in Random and Complex Media ,* vol. 18, no. 1, pp. 151-160, 2008.

[21] C. Fan, M. Pan, F. Luo and B. W. Drinkwater, "Multi-frequency time-reversal-based imaging for ultrasonic nondestructive evaluation using full matrix capture," *IEEE Transactions on Ultrasonics, Ferroelectrics, and Frequency Control,* vol. 61, no. 12, pp. 2067-2074, 2014 .

[22] J. J. Sakurai, " Modern Quantum Mechanics," *Addison, New York,* 1994.

[23] Y. Jie, C. L. Anne, G. Bernhard and H. Fazle, "Inverse scattering theory: Inverse scattering series method for one dimensional non-compact support potential," *J. Math. Phys,* vol. 55, no. 12, p. 123512, 2014.

[24] S. Rienstra and A. Hirschberg, "An introduction to Acoustics," *Eindhoven: Self-publishing,* 2019.

[25] S. Rienstra and B. Teste, "An analytic Greens' function for a lined circular duct containing uniform mean flow," *Journal of Sound and Vibration,* vol. 317, no. 5, pp. 994-1016, 2008.

Preprint not peer reviewed

This preprint research paper has not been peer reviewed. Electronic copy available at: https://ssrn.com/abstract=4841303

[26] T. C. Lin and G. W. Morgan, "Wave Propagation through Fluid Contained in a Cylindrical, Elastic Shell," *The Journal of the Acoustical Society of America,* vol. 28, no. 6, pp. 1165-1176, 1956.

[27] A. J. Devaney and E. A. M. a. F. K. Gruber, "Time-reversal-based imaging and inverse scattering of multiply scattering point targets," *The Journal of the Acoustical Society of America,* vol. 118 , p. 3129, (2005).

[28] S. Fan, A. Zhang, H. Sun and F. Yun, " A Local TR-MUSIC Algorithm for Damage Imaging of Aircraft Structures," *Sensor,* vol. 21, no. 10, p. 3334, 2021.

[29] M. Louati and M. S. Ghidaoui, "High frequency acoustic wave properties in a water-filled pipe. Part 1: Dispersion and multi-path behaviour," *J. Hydraul. Res.,* vol. 55, no. 5, pp. 613-631, 2017.

[30] Z. Lai, M. Louati, S. Nasraoui and M. S. Ghidaoui, "Numerical Investigation of High Frequency Wave-Leak Interaction in Water-Filled Pipes," *J. Hydraul. Eng,* vol. 147, no. 1, p. 04020091, 2021.

Preprint not peer reviewed

This preprint research paper has not been peer reviewed. Electronic copy available at: https://ssrn.com/abstract=4841303